Applied Catalysis B: Environmental 84 (2008) 474–481

Contents lists available at ScienceDirect

Applied Catalysis B: Environmental

journal homepage: www.elsevier.com/locate/apcatb

Synthesis, characterization, redox and photocatalytic properties of $Ce_{1-x}Pd_xVO_4$ ($0 \leq x \leq 0.1$)

Manjunath B. Bellakki [a], Tinku Baidya [a], C. Shivakumara [a], N.Y. Vasanthacharya [a], M.S. Hegde [a], Giridhar Madras [b,*]

[a] Solid State and Structural Chemistry Unit, Indian Institute of Science, Bangalore 560012, India
[b] Chemical Engineering Department, Indian Institute of Science, Bangalore 560012, India

ARTICLE INFO

Article history:
Received 27 February 2008
Received in revised form 25 April 2008
Accepted 7 May 2008
Available online 14 May 2008

Keywords:
Combustion synthesis
$Ce_{0.98}Pd_{0.02}VO_4$
H_2/TPR
NO reduction
CO oxidation
Photocatalysis

ABSTRACT

Zircon-type $CeVO_4$ and $Ce_{1-x}Pd_xVO_4$ ($0.02 \leq x \leq 0.1$) were synthesized by a single step solution combustion method. The materials were characterized by powder X-ray diffraction, magnetic measurement and temperature-programmed reduction (TPR) with H_2. The redox properties of $CeVO_4$ and $Ce_{0.98}Pd_{0.02}VO_4$ have been investigated by temperature-programmed reduction. The gas-phase and liquid-phase catalytic properties of $CeVO_4$ and $Ce_{0.98}Pd_{0.02}VO_4$ were investigated. $Ce_{0.98}Pd_{0.02}VO_4$ shows better catalytic activity than $CeVO_4$ towards CO oxidation by O_2, NO reduction by CO and the photocatalytic degradation of various dyes. This higher catalytic activity of $Ce_{0.98}Pd_{0.02}VO_4$ can be attributed to the lattice labile oxygen and high surface area compared to that of $CeVO_4$.

1. Introduction

Noble metal promoted perovskites have been studied for potential use as automobile exhaust catalysts [1–3]. Incorporation of these metals into a perovskite structure can prevent their sintering, reduce losses due to volatilization at high operating temperatures, and avoid reactions with the support that lead to catalyst deactivation. The need for global and regional environmental protection has strengthened regulations for automobile emission worldwide. Particularly, with the focus on cold emission regulation, the demand for Pd, which shows good low-temperature activity, has increased to 10-fold from 1992. A new automotive catalyst technology that reduces precious metal consumption, especially Pd, is much sought after.

In recent years, vanadia/ceria combination catalysts have been the subject of numerous investigations because of its wide ranging applications in catalysis and material science [4,5]. The naturally occurring $CeVO_4$ mineral wakefieldite crystallizes in a zircon-type (I41/amd) structure that consists of VO_4 tetrahedra sharing corners and edges with CeO_8 dodecahedra [6]. This tetragonal zircon-type structure stabilizes Ce^{3+} ion even in oxidizing conditions [7]. $CeVO_4$ is a highly active catalyst in oxidative dehydrogenation of propane at low temperatures [8]. $CeVO_4$-based materials are used as counter electrodes in electrochromic devices [9]. Moreover, $CeVO_4$-based phases are of great interest for high-temperature electrochemical applications because of the significant ionic and electronic conductivity [10]. The conventional methods for the preparation of rare earth orthovanadates include solid-state reaction [7,11], coprecipitation [12], nitrate method [8], hydrothermal method [13], sonochemical method [14] and using microwave radiation [15].

Ionic substitution of noble metals in CeO_2 in the form of $Ce_{1-x}M_xO_{2-\delta}$ ($M = Pd^{2+}$) results in high catalytic activity of these materials towards three-way catalysis [16]. $Ce_{1-x}Ti_xO_2$ can be prepared retaining fluorite structure and Ce^{4+}/Ce^{3+} and Ti^{4+}/Ti^{3+} redox couples can be accessed [17]. Vanadium ion substitution with stable $V^{5+}/V^{4+}/V^{3+}$ in CeO_2 is not possible because the stable phase of $CeVO_4$ is formed instead. However, Ce^{3+}/Ce^{4+} and V^{5+}/V^{4+} redox states can be accessed in $CeVO_4$ and noble metal ion substitution in $CeVO_4$ can result in beneficial effects for redox catalysis. This idea motivated us to synthesize Pd ion-substituted $CeVO_4$ and test its catalytic activity for both gas-phase and liquid-phase reactions.

The present catalysts were synthesized by solution combustion method. Solution combustion method offers an advantage over the

* Corresponding author. Tel.: +91 80 2293 2321; fax: +91 80 2360 0683.
E-mail addresses: giridhar@chemeng.iisc.ernet.in, giridharmadras@gmail.com (G. Madras).

0926-3373/$ – see front matter © 2008 Elsevier B.V. All rights reserved.
doi:10.1016/j.apcatb.2008.05.001

other conventional methods. It is a low-temperature initiated exothermic and self-propagating process. Patil et al. [18] have reviewed synthesis of various oxide materials by the combustion reactions of redox mixtures containing stoichiometric amounts of respective metal nitrates (oxidisers) and various fuels. A wide range of technologically useful oxides can be prepared using this technique.

The exhaust gases from vehicle engines and industrial boilers contain mainly carbon oxides, nitrogen oxide and hydrocarbons that are major contributors to environmental problems like smog and acid rain [19,20]. Extensive research has been carried out on NO reduction to N_2 with CO, as summarized in a review [21]. The widespread presence of organic dyes in industrial wastewater results in a potentially serious environmental problem. Photocatalysis is a promising technology to treat wastewater and extensive studies have been reported on the degradation of dyes, as summarized in review [22].

Thus the objectives of this study are to synthesize and characterize $Ce_{1-x}Pd_xVO_4$ ($0 \leq x \leq 0.1$), determine its catalytic activity for both gas phase (CO oxidation and NO reduction) and liquid phase reactions (photocatalysis of dyes). Further, this study provides a rationale for the higher activity of $Ce_{1-x}Pd_xVO_4$ compared to that of $CeVO_4$.

2. Experimental

2.1. Preparation of catalysts

$CeVO_4$ was prepared by taking stoichiometric amounts of $(NH_4)_2Ce(NO_3)_6{\cdot}6H_2O$ (E. Merck, India Ltd.), NH_4VO_3('Reanal' Finom vegyszergyar Budapest-Hungary) and oxalyl dihydrazide fuel (ODH, prepared by the reaction of 1 mol of diethyl oxalate and 2 mol of hydrazine hydrate). In a typical preparation of $CeVO_4$, 9.12 mmol of $(NH_4)_2Ce(NO_3)_6{\cdot}6H_2O$, 9.12 mmol of NH_4VO_3 and 24.63 mmol of ODH, were taken in a borosilicate dish of 130 cm^3 capacity. The reactants were dissolved in 20 ml water and introduced into a preheated muffle furnace at 500 °C. The solution boiled with frothing, foaming and ignited to burn with a flame (~1000 °C) yielding a voluminous solid product. The chemical reaction occurring in the combustion process can be written as

$$2(NH_4)_2Ce(NO_3)_6 + 2NH_4VO_3 + 3C_2H_6N_4O_2 \rightarrow 2CeVO_4 + 6CO_2 + 15N_2 + 21H_2O + (7/2)O_2$$

$Ce_{0.98}Pd_{0.02}VO_4$ was synthesized by taking $(NH_4)_2Ce(NO_3)_6{\cdot}6H_2O$, $PdCl_2$, NH_4VO_3 and ODH in the mole ratio of 0.98:0.02:1.0:2.65. In typical reaction, 9.12 mmol of $(NH_4)_2Ce(NO_3)_6{\cdot}6H_2O$, 9.31 mmol of NH_4VO_3, 0.31 mmol of palladium chloride and 49.36 mmol of ODH were used.

2.2. Impregnation method

A known amount of combustion synthesized $CeVO_4$ was wetted with water and calculated quantity of $PdCl_2$ was added dropwise with gentle stirring. The mixture was then dried at 100 °C and finally calcined in air at 500 °C for 6 h.

2.3. Characterization of catalysts

Powder X-ray diffraction (XRD) patterns of the synthesized oxides were recorded on a Philips X'Pert X-ray diffractometer with Cu Kα source (λ = 1.5418 Å) at a scan rate of 0.5°/min with 0.02 step size in the 2θ range 10–80°. Rietveld refinement of the structures was carried out using Fullprof program.

X-ray photoelectron spectra (XPS) of $Ce_{1-x}Pd_xVO_4$ was recorded in ESCA-3 II spectrometer (VG Scientific Ltd., England) using Al Kα radiation (1486.6 eV). Binding energies were calibrated with respect to C(1s) at 285 eV with a precision of ±0.1 eV. For XPS analysis, the powder samples were made into 0.5-mm thick, 8 mm diameter pallets and placed into an ultra high vacuum (UHV) chamber at 10^{-9} Torr housing the analyzer.

Hydrogen uptake studies were carried out in a temperature-programmed reduction (TPR) system with 5% H_2/Ar. About 100 mg of sample in a granular form (40–80 mesh powder) was placed in a fixed bed tubular reactor, over which 5% H_2 in Ar was continuously passed. The samples were subjected to a heating rate of 10 °C min^{-1}. The volume of hydrogen uptake, calibrated against a known amount of CuO, was measured using a TCD detector.

The surface area of the catalyst was determined with standard BET apparatus (NOVA-1000, Quantachrome) using nitrogen for adsorption at 77 K. Experiments were carried out in multipoint BET mode.

UV–vis absorption spectra and the diffuse reflectance spectra of $CeVO_4$ and $Ce_{0.98}Pd_{0.02}VO_4$ were determined using a spectrophotometer (Lambda 32, PerkinElmer).

2.4. Catalytic tests

The catalytic reaction was carried out in a TPR system in a packed bed tubular quartz reactor (25 cm × 0.4 cm) at atmospheric pressure. The system was equipped with a quadrupole mass spectrometer SX200 (VG Scientific Ltd., England) for product analysis. Typically, 250 mg of the catalyst (40/80 mesh size) diluted with SiO_2 (30/60 mesh size) was loaded in the reactor to obtain a column length of 2.2 cm and the ends were plugged with ceramic wool. For all the reactions, the total flow was maintained at 100 sccm to achieve a gas hourly space velocity (GHSV) of 15,000 h^{-1}. Before the catalytic experiments, the as-prepared catalyst was heated in O_2 flow at 200 °C for 1 h followed by degassing in He flow to the experimental temperature. The reactions were carried out as a function of temperature with a linear heating rate of 10 °C/min. In order to check for mass transfer effects, experiments were also conducted with lower heating rates of 2–5 °C/min but similar reaction rates were obtained. Experiments were also conducted using the once used catalyst and no deactivation of the catalyst was observed.

2.5. Photochemical reactor

The details of the photochemical reactor employed in this study have been reported elsewhere [23]. A high-pressure mercury vapor lamp (HPML) (125 W, Philips, India) that radiated predominantly at 365 nm corresponding to the energy of 3.4 eV was used for the degradation reactions.

2.6. Degradation and sample analysis

The photocatalytic degradation of four dyes having chemical structures such as azoic (Orange G, OG), sulfonated (Remazol brilliant blue, RBBR), heteropolyaromatic (Methylene blue, MB) and anthraquinonic (Alizarin red, AR) was investigated in the presence of $CeVO_4$ and $Ce_{0.98}Pd_{0.02}VO_4$. The degradation reactions were performed in a photochemical reactor with a constant catalyst concentration of 1 g/l. The reactions were carried out at natural pH conditions with the initial concentrations of 50 ppm. Samples were collected at regular intervals for subsequent analysis. Experiments were also conducted in the presence of commercial catalyst, TiO_2 (Degussa P-25).

The degraded samples were centrifuged and filtered through Millipore membrane filters to remove the catalyst particles prior to analysis. The samples were analyzed using a UV–visible spectro-

photometer (Lambda 32, PerkinElmer). The calibrations for OG, RBBR, AR and MB were based on Beer Lambert's Law at their maximum absorption wavelengths λ_{max} of 480, 590, 428 and 664 nm, respectively.

3. Results and discussion

3.1. Structural studies

The powder XRD pattern of $CeVO_4$ and $Ce_{1-x}Pd_xVO_4$ ($0.02 \leq x \leq 0.1$) solid solutions are shown in Fig. 1. The XRD patterns can be indexed to zircon-type structure ($ZrSiO_4$). The diffraction patterns agree well with the reported pattern in the literature (JCPDS No. 12-0757). The compounds crystallize in the same $CeVO_4$ structure up to 2% Pd. To see if any impurity line of PdO is present in 2 at.% Pd-substituted $CeVO_4$ compounds, we have given the enlarged powder XRD pattern of (a) $Ce_{0.98}Pd_{0.02}VO_4$ by combustion method, (b) 2 at.% Pd-impregnated $CeVO_4$ and (c) 2 at.% PdO mixed $CeVO_4$ in Fig. 2. As can be seen from Fig. 2(a), combustion synthesized $Ce_{0.98}Pd_{0.02}VO_4$ giving almost no PdO(1 0 1) peak. Also Pd metal peaks are absent. The impurity line of PdO (1 0 1) was observed in both 2 at.% Pd-impregnated $CeVO_4$ and 2 at.% PdO mixed $CeVO_4$ as can be seen in Fig. 2(b) and (c), respectively. In the XRD pattern of $Ce_{0.95}Pd_{0.05}VO_4$ and $Ce_{0.90}Pd_{0.10}VO_4$ compounds, weak reflections due to PdO are observed (see Fig. 1). To see whether PdO is present in the combustion synthesized 3 at.% Pd/$CeVO_4$, the *X* and *Y* scale expanded XRD pattern was examined along with 3 at.% PdO + $CeVO_4$. A small amount of impurity line PdO(1 0 1) was observed (Fig. S1(a)). The intensity of PdO(1 0 1) in the combustion synthesized 3 at.% Pd/$CeVO_4$ is very less compared to 3 at.% PdO mixed with $CeVO_4$(see Fig. S1(b)). Thus we have chosen only 2% Pd/$CeVO_4$ for catalytic studies even though we have prepared 3% Pd/$CeVO_4$, 5% Pd/$CeVO_4$ and 10% Pd/$CeVO_4$. Our interest is to show how much Pd can be substituted as Pd^{2+} ion in $CeVO_4$. In the present study we have focused on the catalytic activity of $CeVO_4$ and 2% Pd-substituted $CeVO_4$ by combustion method, where Pd exists as a Pd^{2+}. The XRD pattern of $CeVO_4$ is Rietveld refined and the profile fits well to tetragonal zircon-type structure (space group $I4_1/amd$), as shown in Fig. S2. The XRD pattern of all the Pd-substituted compounds are Rietveld refined and profile fits well to tetragonal zircon-type structure as shown in Fig. S3 (a–d). The refined parameters are given in Table S1 (see supporting information). Based on Rietveld refined data (accurate to two decimals), cell volume of 2 at.% Pd/$CeVO_4$ (combustion) is 356.66 (Å^3), 2 at.% Pd-impregnated $CeVO_4$ is 356.85 (Å^3) and 2 at.% PdO + $CeVO_4$ is 356.18 (Å^3). Thus, by XRD, it clear that Pd ion is in the lattice.

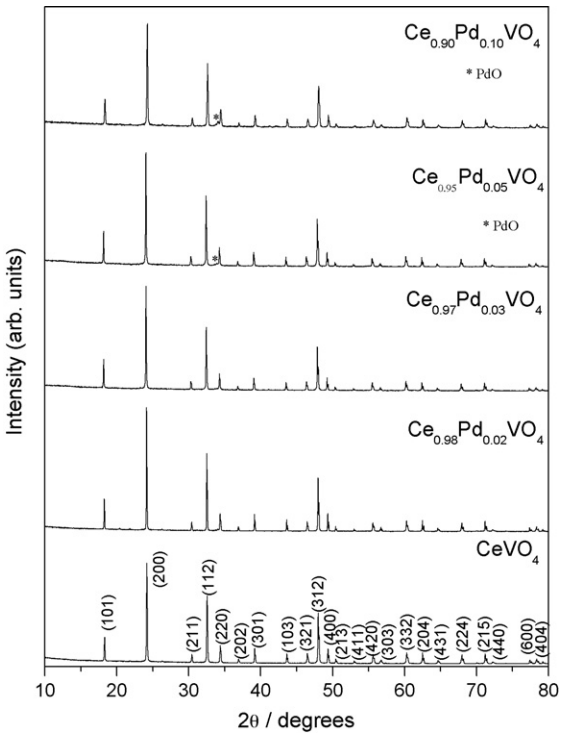

Fig. 1. Powder XRD patterns of $CeVO_4$, $Ce_{0.98}Pd_{0.02}VO_4$, $Ce_{0.97}Pd_{0.03}VO_4$, $Ce_{0.95}Pd_{0.05}VO_4$ and $Ce_{0.90}Pd_{0.10}VO_4$.

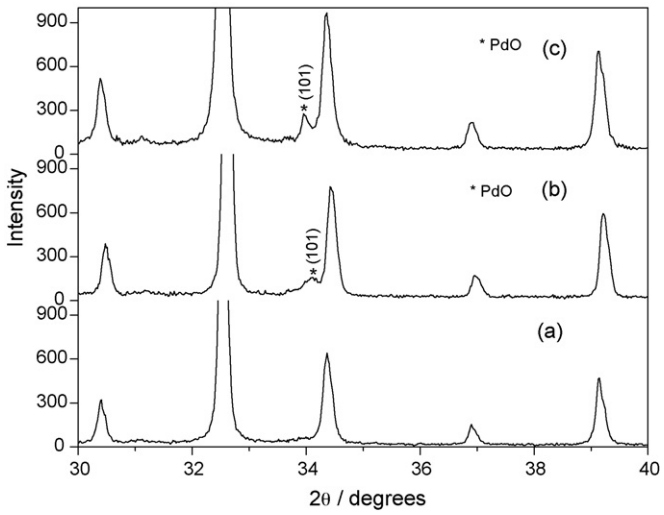

Fig. 2. Enlarged powder XRD patterns of (a) $Ce_{0.98}Pd_{0.02}VO_4$, (b) 2 at.% Pd/$CeVO_4$ (impreg.) and (c) 2 at.% PdO/$CeVO_4$.

Powder XRD patterns of (a) as synthesized $CeVO_4$, (b) reduced $CeVO_4$ to $CeVO_3$ under H_2 atmosphere at 800 °C and (c) reoxidised $CeVO_3$ to $CeVO_4$ are shown in Fig. 3. Fig. 3(b) shows the XRD pattern of $CeVO_3$ recorded after H_2 was passed over $CeVO_4$ from 30 °C to 900 °C. $CeVO_3$ crystallized in the orthorhombic structure (JCPDS No. 78-2306). Fig. 3(c) shows the XRD pattern of $CeVO_4$ obtained on reoxidation of $CeVO_3$ in air. The Rietveld refined XRD pattern of $CeVO_3$ fits well to orthorhombic structure with *Pbnm*

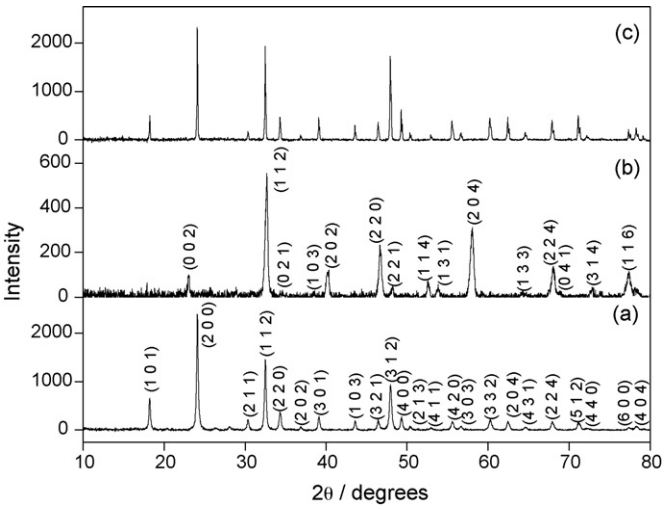

Fig. 3. Powder XRD patterns of (a) as-synthesized $CeVO_4$, (b) reduced $CeVO_4$ to $CeVO_3$ under H_2 atmosphere at 800 °C and (c) reoxidised $CeVO_3$ to $CeVO_4$.

space group shown in Fig. S4. The black $CeVO_3$ compound turns to pinkish brown colour and the structure is restored to $CeVO_4$ (Fig. 3(c)). The overall redox behavior can be represented as follows:

$$CeVO_4 + H_2 \rightarrow CeVO_3 + H_2O$$

$$CeVO_3 + (1/2)O_2 \rightarrow CeVO_4$$

X-ray photoelectron spectra of Pd ion-substituted $CeVO_4$ have been recorded to determine the electronic structure. Fig. 4(a) shows the core level spectra of Pd($3d_{5/2}$) in $Ce_{0.98}Pd_{0.02}VO_4$. Binding energy of Pd($3d_{5/2}$) is 337.7 eV which is higher than that in PdO at 336.4 eV [24]. Therefore, Pd cannot be present in the PdO form. Hence, Pd^{2+} ion must be present in $Ce_{0.98}Pd_{0.02}VO_4$ lattice giving higher binding energy of Pd(3d) core level.

Fig. 4(b) shows that the characteristic satellite peak of Ce(3d) spectrum is similar to Ce_2O_3 [25]. Therefore, Ce ion in $CeVO_4$ is in +3 state (*) in $Ce_{0.98}Pd_{0.02}VO_4$ and a very small amount in +4 state (+). V($2p_{3/2}$) peak is observed at 517.2 eV, while O(1s) is observed at 529.6 eV indicating that vanadium is in +5 state as seen from Fig. 4(c).

UV–vis absorption (and diffuse reflectance) spectra of $CeVO_4$ and Pd/$CeVO_4$ shows optical threshold at 586 and 595 nm, respectively (Fig. 5), corresponding to band gaps of 2.12 and 2.08 eV, respectively.

The magnetic susceptibility measurement was performed in the temperature range of 10–300 K under 20 kOe. Fig. 6 shows the variation χ_m^{-1} with temperature for $CeVO_4$ and $Ce_{0.98}Pd_{0.02}VO_4$. The susceptibility of $CeVO_4$ and $Ce_{0.98}Pd_{0.02}VO_4$ follows the Curie–Weiss (C–W) law quite well from 300 K down to nearly 75 K. At low temperatures, both $CeVO_4$ and $Ce_{0.98}Pd_{0.02}VO_4$ exhibit a strong deviation from the Curie–Weiss law and the curve bends downward. This anomalous behavior has also been observed for other cerium compounds [26–28]. The magnetic moment measured for $CeVO_4$ is 2.51μ_B, which agrees well with Ce in +3 state ($4f^1$) of

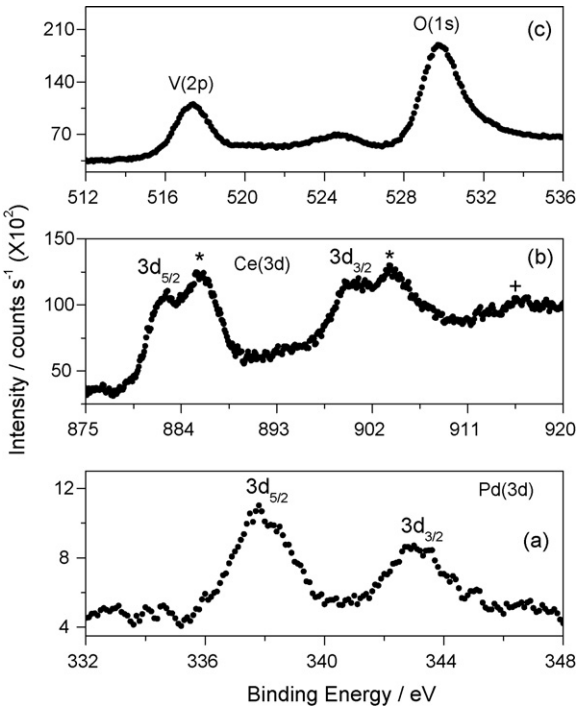

Fig. 4. XPS of (a) Pd(3d) core level in $Ce_{0.98}Pd_{0.02}VO_4$, (b) XPS of Ce(3d) core level in $Ce_{0.98}Pd_{0.02}VO_4$. (*) Sign indicates Ce^{3+} satellite peak and (+) sign for Ce^{4+} satellite peak (c) XPS of V(3d) core level in $Ce_{0.98}Pd_{0.02}VO_4$.

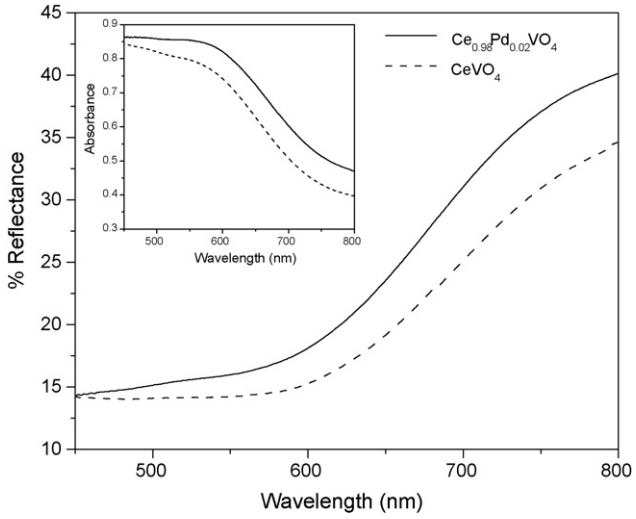

Fig. 5. UV–vis diffuse reflectance spectra of $CeVO_4$ and $Ce_{0.98}Pd_{0.02}VO_4$.

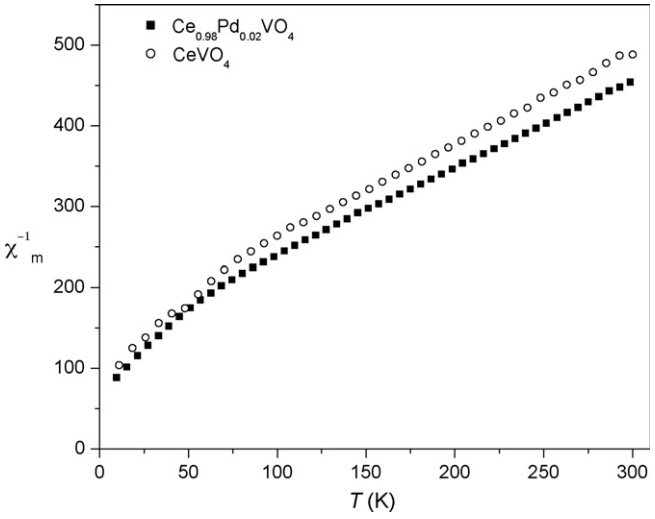

Fig. 6. Magnetic Susceptibility of $CeVO_4$ and $Ce_{0.98}Pd_{0.02}VO_4$.

2.54μ_B [29]. In case of $Ce_{0.98}Pd_{0.02}VO_4$, the susceptibility value is 2.65μ_B, which is higher than $CeVO_4$. This is attributed to isolated Pd^{2+} ion substitution for Ce^{3+} sites.

3.2. Hydrogen uptake studies

Hydrogen uptake of the pure oxide and its corresponding Pd-substituted compounds were carried out to investigate the influence of Pd ion substitution. Fig. 7 shows the TPR profiles of $CeVO_4$ and $Ce_{1-x}Pd_xVO_4$ (x = 0.02 and 0.03). The H_2/TPR profile of $CeVO_4$ shows two peaks with a weak shoulder at 560 °C, which has been attributed to surface V^{5+} reduction followed by bulk vanadium ion (V^{5+}) reduction peak at 760 °C. The area under the peak up to 900 °C corresponds to 98 cm^3 of H_2 per gram of $CeVO_4$. The H_2 reduction temperature of $CeVO_4$ to $CeVO_3$ agrees well with that reported by Varma et al. [11].

H_2 uptake starts at ~50 °C in $Ce_{0.98}Pd_{0.02}VO_4$ with a small hydrogen adsorption peak at ~110 °C and a main peak at 760 °C due to vanadium reduction is observed. The peak corresponding to surface V^{5+} to V^{3+} ion reduction in $CeVO_4$ is absent in $Ce_{0.98}Pd_{0.02}VO_4$. The H_2 uptake peak can be attributed to Pd^{2+} ion reduction. Taking

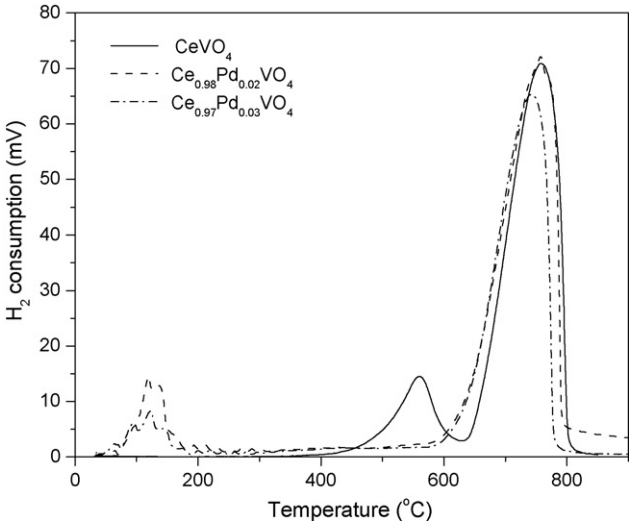

Fig. 7. H_2 TPR profile of $CeVO_4$, $Ce_{0.98}Pd_{0.02}VO_4$ and $Ce_{0.97}Pd_{0.03}VO_4$.

only the area under the low temperature H_2 peak at 110 °C, the ratio of H/Pd is 12 in $Ce_{0.98}Pd_{0.02}VO_4$. H/Pd ratio should have been 2 if we consider only $PdO + H_2 \rightarrow Pd + H_2O$ reaction. Therefore, higher H/Pd at lower temperature is due to reduction of Pd^{2+} to Pd° as well as the reduction of V^{5+} to V^{3+}. Thus Pd^{2+} ion substitution in $CeVO_4$ induces significant amount of V^{5+} ion reduction at a lower temperature. Further, we have varied the Pd ion concentration in $CeVO_4$ to see its effect on reduction of V^{5+} to V^{3+} at lower temperature. Taking the area under the low temperature H_2 peak at 110 °C, the ratio of H/Pd is 3.5 in $Ce_{0.97}Pd_{0.03}VO_4$ which is attributed to some extent of surface reduction of V^{5+} to V^{3+} ion along with PdO reduction. The main V^{5+} ion reduction peak shifts to lower temperature as compared to pure $CeVO_4$.

3.3. CO oxidation by O_2

CO oxidation has been studied in the presence of Pd-supported oxides [30–32]. CO oxidation was carried out with $CO:O_2$ ratio of 1:0.5 vol%. Fig. 8(a) shows the CO oxidation profile over 250 mg of $CeVO_4$, 2 at.% Pd-impregnated $CeVO_4$ and $Ce_{0.98}Pd_{0.02}VO_4$ with T_{50} at 540, 290 and 235 °C, respectively. The rates and activation energies of $CO + O_2$ reaction over $CeVO_4$ and $Ce_{0.98}Pd_{0.02}VO_4$ have been calculated. Rate is defined as, $F_{CO}x/W$ where F_{CO} is the molar flow rate (mol/s), W is the weight of the catalyst (g) and x is the fractional conversion. Experiments were also conducted by varying the weight of the catalyst (W = 50, 100, 150 and 250 mg) and the rates were taken from the linear region (less than 20% conversion) of the W/F versus conversion plot. Fig. 8(b) shows the Arrhenius plot for the $CO + O_2$ reaction in the presence of $CeVO_4$ and $Ce_{0.98}Pd_{0.02}VO_4$. The plot represents experimental data up to 15% CO conversion. The activation energy of CO oxidation over $Ce_{0.98}Pd_{0.02}VO_4$ is 54.4 kJ/mol, which is lower than that observed over $CeVO_4$ (125.5 kJ/mol). Thus, $Ce_{0.98}Pd_{0.02}VO_4$ shows better catalytic activity compared to $CeVO_4$. Further, this activation energy is also considerably lower than other Pd-substituted catalysts like 0.5 wt% Pd/CeO_2–ZrO_2 catalyst (175 kJ/mol) [33], 5 wt% Pd/SiO_2(103 kJ/mol) [34], $Pd/CeO_2/Al_2O_3$ (84 kJ/mol) [35].

To confirm whether 2 at.% $Pd/CeVO_4$ prepared by impregnation method has a different catalytic activity compared to 2% Pd-substituted $CeVO_4$ by combustion method. We carried out CO oxidation on this material with $CO:O_2$ ratio of 1:0.5 vol%. Fig. 8(a) shows the CO oxidation profile over 250 mg of 2 at.% $Pd/CeVO_4$ (impreg.) and $Ce_{0.98}Pd_{0.02}VO_4$. The T_{50} for Pd-impregnated $CeVO_4$ and Pd-substituted $CeVO_4$ are 290 and 235 °C respectively, indicating that combustion synthesized $Pd/CeVO_4$ has higher activity than $CeVO_4$ and Pd-impregnated $CeVO_4$.

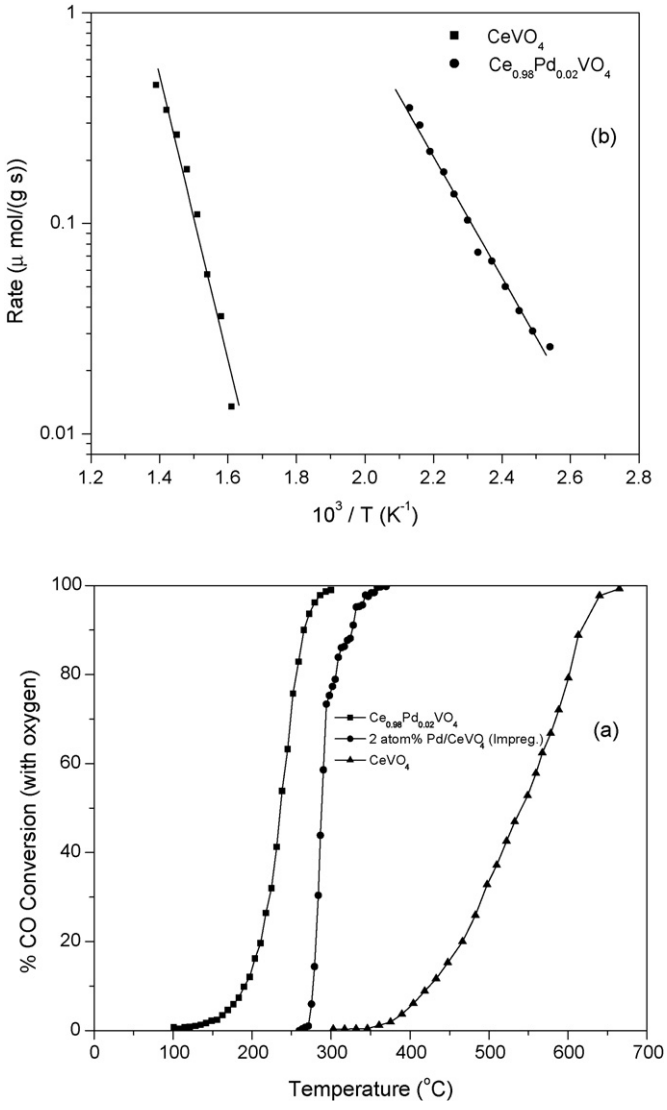

Fig. 8. (a) %CO conversion as a function of temperature over $CeVO_4$, 2 at.% $Pd/CeVO_4$ (impreg.) and $Ce_{0.98}Pd_{0.02}VO_4$ under the reaction condition: CO = 1 vol%, O_2 = 0.5 vol%, F_t = 100 sccm, GHSV = 15,000 h^{-1}, W = 250 mg. (b) Rate vs. temperature from W/F_{CO} plot for $CeVO_4$ and $Ce_{0.98}Pd_{0.02}VO_4$.

To check the availability of lattice oxygen, we also carried out CO oxidation without a stream of oxygen (O_2). The reaction was carried out by passing 0.5 vol% CO in He with total flow of 100 cm^3/min. In this experiment, we have used lower concentration of CO and higher amount of catalyst to observe the conversion significantly up to sufficiently high temperature. There is no possibility of CO_2 formation from CO decomposition because that process is highly endothermic in nature. Therefore, CO_2 is formed only utilizing oxygen from the lattice. Fig. 9 shows the CO oxidation profile in the presence of $CeVO_4$ and $Ce_{0.98}Pd_{0.02}VO_4$. About 70% CO conversion occurs with both $CeVO_4$ and $Ce_{0.98}Pd_{0.02}VO_4$. 50% CO conversion is observed at ~230 and ~530 °C for $Ce_{0.98}Pd_{0.02}VO_4$ and $CeVO_4$, respectively. Pd acts as an adsorption active site for CO oxidation therefore, conversion occurs at lower temperature in $Ce_{0.98}Pd_{0.02}VO_4$ compared to that of $CeVO_4$. Clearly, lattice oxygen is more labile in $Ce_{0.98}Pd_{0.02}VO_4$ than $CeVO_4$. Further the temperature at which CO oxidation occurs over

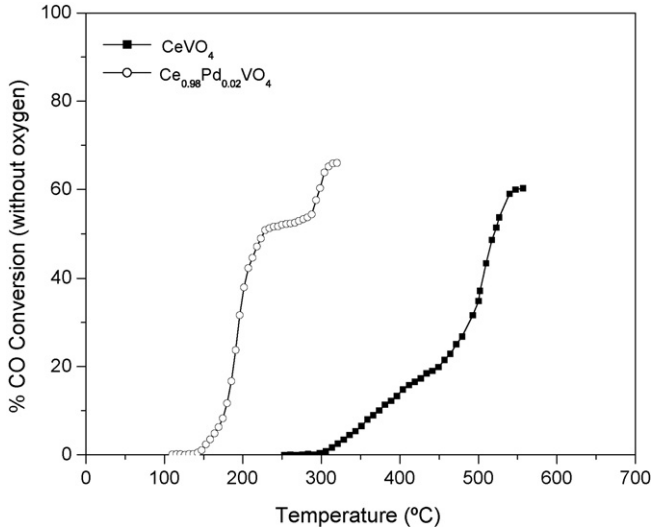

Fig. 9. %CO conversion as a function of temperature over $CeVO_4$ and $Ce_{0.98}Pd_{0.02}VO_4$, without oxygen.

$Ce_{0.98}Pd_{0.02}VO_4$ agrees well with H_2 uptake peak. Thus, lattice oxygen from Pd ion-substituted $CeVO_4$ is labile for CO oxidation.

In $CeVO_4$, Ce is in reduced state and V^{5+}/V^{3+} or V^{5+}/V^{4+} redox couple is observed instead of Ce^{4+}/Ce^{3+} couple, as observed from $CeVO_4$ to $CeVO_3$ conversion (Fig. 3). In this compound, V^{5+}/V^{3+} redox reaction occurs at high temperature ~750 °C, as seen from H_2/TPR profile. Pd^{2+} ion substitution induces reduction of V^{5+} to V^{4+}/V^{3+} to a lower temperature only partially as seen from H/Pd ratio of 12 and thus CO oxidation either with lattice oxygen or with stream oxygen occurs at a lower temperature over $Ce_{0.98}Pd_{0.02}VO_{2-\delta}$ than $CeVO_4$.

3.4. NO reduction by CO

NO reduction by CO has been studied in the presence of Pd-supported oxides [36–38]. NO reduction by CO was carried out with NO:CO (0.5:0.5) with 100 sccm total flow over 250 mg of $CeVO_4$ and $Ce_{0.98}Pd_{0.02}VO_4$ catalysts is shown. In Fig. 10(a), TPR profile of NO + CO over $CeVO_4$ and $Ce_{0.98}Pd_{0.02}VO_4$ catalysts is given. In unsubstituted $CeVO_4$, 50% NO conversion was observed at 650 °C, while in the case of $Ce_{0.98}Pd_{0.02}VO_4$, 50% conversion occurs at 280 °C and 100% conversion at 350 °C. Thus it indicates that Pd ion-substituted $CeVO_4$ is more active than $CeVO_4$. This is due to ionically dispersed Pd in $CeVO_4$ lattice, which gives rise to oxygen vacancy. The oxide ion vacancies in the catalyst are created due to Pd^{2+} ionic substitution, as confirmed by the XPS studies. Fig. 10(b) shows the Arrhenius plot for the NO reduction by CO in the presence of $CeVO_4$ and $Ce_{0.98}Pd_{0.02}VO_4$. The experimental data in the plot is restricted to 15% NO conversion. The activation energies are 90 and 148 kJ mol^{-1} for $Ce_{0.98}Pd_{0.02}VO_4$ and $CeVO_4$, respectively indicating that $Ce_{0.98}Pd_{0.02}VO_4$ is a better catalyst than $CeVO_4$. Further, this activation energy is very similar to other Pd-substituted catalysts like, 1 at.% Pd/Al_2O_3 (86.6 kJ/mol) [38], 4.12 wt% $Pd/CeO_2/Al_2O_3$ (77 kJ/mol) [39], $Pd/Mo/Al_2O_3$ (84 kJ/mol) [40].

3.5. Photocatalysis

Photocatalytic reactions have been studied in the presence of Pd-supported oxides [41–44]. The photocatalytic degradation of azoic, sulfonated, heteropolyaromatic and anthraquinonic dyes was investigated. Fig. 11(a–d) shows normalized degradation

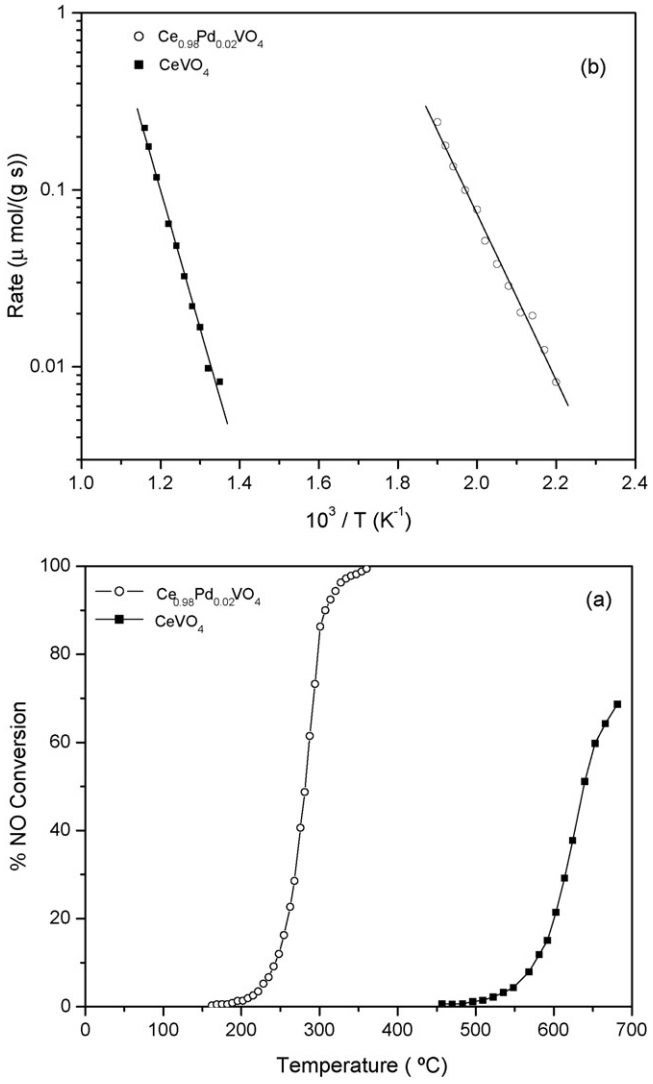

Fig. 10. (a) %NO conversion vs. temperature for the reaction NO + CO under the condition: NO = 0.5 vol%, CO = 0.5 vol%, F_t = 100 sccm, GHSV = 15,000 h^{-1}, W = 250 mg. (b) Rate vs. temperature from W/F_{NO} plot for $CeVO_4$ and $Ce_{0.98}Pd_{0.02}VO_4$.

profiles of all the four dyes in the presence of both $CeVO_4$ and $Ce_{0.98}Pd_{0.02}VO_4$. The degradation profiles are comparable to the degradation rate in the presence of commercial TiO_2 (Degussa P-25). Similar results were obtained for the degradation of methylene blue in the presence of $CeVO_4$ synthesized by the conventional solution technique [45]. The concentration of the dye levels off at long times and no further degradation occurs. In order to verify whether this is due to the deactivation of the catalyst, experiments were conducted with the catalyst and then the once used catalyst was used again for the degradation experiment. It was found that the catalyst had similar activity in subsequent experiments indicating that catalyst deactivation has not occurred.

The degradation rate of all the dyes in the presence of $Ce_{0.98}Pd_{0.02}VO_4$ was found to be faster than in the presence of $CeVO_4$. This indicates Pd-substituted $CeVO_4$ is more active than $CeVO_4$. The difference in degradation rates of the dyes in the presence of $CeVO_4$ and $Ce_{0.98}Pd_{0.02}VO_4$ cannot be attributed to band gaps because these materials have similar band gaps (2.12 eV for $CeVO_4$ and 2.08 eV for $Ce_{0.98}Pd_{0.02}VO_4$). However, surface area of $CeVO_4$ and $Ce_{0.98}Pd_{0.02}VO_4$ are 3 and 19 m^2/g, respectively. Further, the lattice oxygen from Pd ion-substituted $CeVO_4$ is more

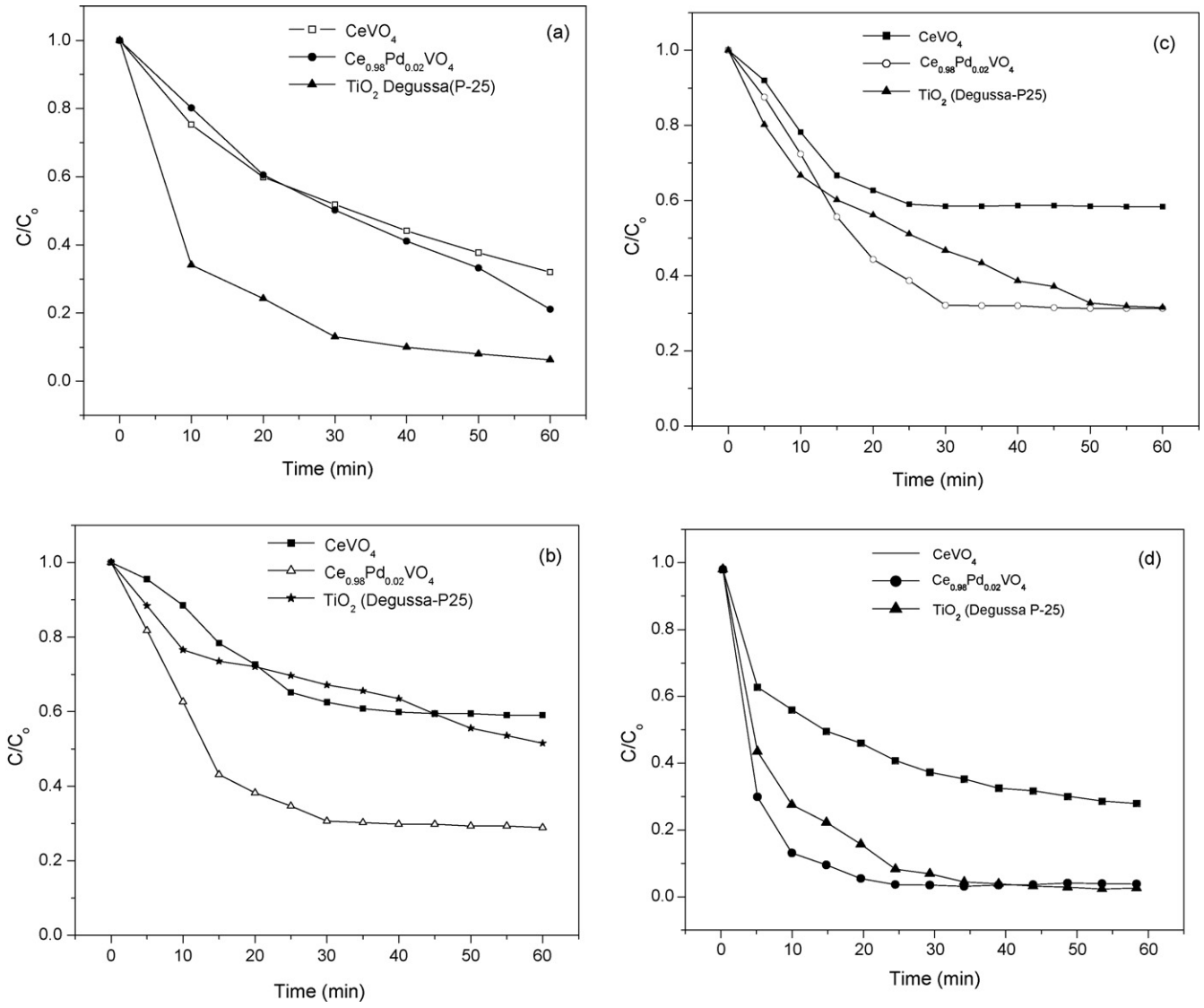

Fig. 11. Photocatalytic degradation profiles of the dyes, (a) Methylene blue, MB (b) Remazol brilliant blue, RBBR (c) Orange (G) and (d) Alizarin red (S) in the presence of $CeVO_4$, TiO_2 (Degussa P-25) and $Ce_{0.98}Pd_{0.02}VO_4$.

labile for oxidation of dyes. Thus, $Ce_{0.98}Pd_{0.02}VO_4$ has higher photocatalytic activity than $CeVO_4$.

4. Summary and conclusions

$CeVO_4$ and $Ce_{1-x}Pd_xVO_4$ ($0.02 \leq x \leq 0.1$) were synthesized by a single step solution combustion method for the first time. The materials were characterized by a wide variety of techniques. The gas-phase and liquid-phase catalytic properties of $CeVO_4$ and $Ce_{0.98}Pd_{0.02}VO_4$ were investigated. $Ce_{0.98}Pd_{0.02}VO_4$ shows higher catalytic activity than $CeVO_4$ for CO oxidation by O_2 as well as NO reduction by CO and photodegradation of dyes. This high catalytic activity of $Ce_{0.98}Pd_{0.02}VO_4$ was attributed to the lattice oxygen and high surface area compared to that of $CeVO_4$.

The NO reduction by CO is a site specific reaction wherein conversions would be significant if CO is molecularly adsorbed and NO is dissociatively chemisorbed. The substitution of noble metals in their ionic form in the reducible support leads to higher metal dispersion in ionic form and creation of oxide ion vacancies. In case of Pt-substituted CeO_2 and Pt-substituted TiO_2, the noble metal ion is an adsorbent for CO while the dissociation of NO occurs on the oxide ion vacancy. This leads to higher activity and N_2 selectivity on the noble metal substituted material prepared by combustion synthesis technique compared to noble metal-impregnated material [46]. Similarly, in this study, Pd-substituted $CeVO_4$ shows higher catalytic activity than Pd-impregnated $CeVO_4$.

Acknowledgement

The authors gratefully acknowledge financial support from the Department of Science and Technology, Government of India.

Appendix A. Supplementary data

Supplementary data associated with this article can be found, in the online version, at doi:10.1016/j.apcatb.2008.05.001.

References

[1] W.F. Libby, Science 171 (1971) 499–500.
[2] D.B. Meadowcroft, Nature 226 (1970) 847–848.

[3] R.J.H. Voorhoeve, D.W. Johnson Jr., Science 195 (1977) 827–833.
[4] T. Radhika, S. Sugunan, J. Mol. Catal. A: Chem. 250 (2006) 169–176.
[5] J.M. Vohs, T. Feng, G.S. Wong, Catal. Today 85 (2003) 303–309.
[6] B.C. Chakoumakos, M.M. Abraham, L.A. Boatner, J. Solid State Chem. 109 (1994) 197–202.
[7] A. Watanabe, J. Solid State Chem. 153 (2000) 174–179.
[8] Z.M. Fang, Q. Hong, Z.H. Zhou, S.J. Dai, W.Z. Weng, H.L. Wan, Catal. Lett. 61 (1999) 39–44.
[9] G. Picardi, F. Varsano, F. Decker, U. Opara-Krasovec, A. Surca, B. Orel, Electrochim. Acta. 44 (1999) 3157–3164.
[10] E.V. Tsipis, M.V. Patrakeev, V.V. Kharton, N.P. Vyshatko, J.R. Frade, J. Mater. Chem. 12 (2002) 3738–3745.
[11] S. Varma, B.N. Wani, N.M. Gupta, Mater. Res. Bull. 37 (2002) 2117–2127.
[12] A. Huignard, V. Buissette, G. Laurent, T. Gacoin, J.P. Boilot, Chem. Mater. 14 (2002) 2264–2269.
[13] F. Luo, C.-J. Jia, W. Song, L.-P. You, C.-H. Yan, Crys. Growth Des. 5 (2005) 137–142.
[14] Z. Ling, L. Qin, L. Jiayan, L. Xiangdong, M. Jian, C. Xueqiang, J. Nanoparticle Res. 9 (2007) 261–268.
[15] H. Wang, Y. Meng, H. Yan, Inorg. Chem. Commun. 7 (2004) 553–555.
[16] S. Roy, A. Marimuthu, M.S. Hegde, G. Madras, Appl. Catal. B: Environ. 71 (2007) 23–31.
[17] G. Dutta, U.V. Waghmare, T. Baidya, M.S. Hegde, K.R. Priolkar, P.R. Sarode, Chem. Mater. 18 (2006) 3249–3256.
[18] K.C. Patil, S.T. Aruna, S. Ekambaram, Curr. Opin. Solid State Mater. Sci. 2 (1997) 158–165.
[19] K. Saito, S. Ichihara, Catal. Today 10 (1991) 45–46.
[20] M. Iwamoto, H. Hamada, Catal. Today 10 (1991) 57–71.
[21] A. Fritz, V. Pitchon, Appl. Catal. B: Environ. 13 (1997) 1–25.
[22] M.R. Hoffmann, S.T. Martin, W. Choi, D.W. Bahnemann, Chem. Rev. 95 (1995) 69–96.
[23] G. Sivalingam, K. Nagaveni, M.S. Hegde, G. Madras, Appl. Catal. B: Environ. 45 (2003) 23–28.
[24] D. Briggs, M.P. Seah, Practical Surface Analysis by Auger and X-ray Photoelectron Spectroscopy, John Wiley and Sons Ltd., London 1984.
[25] A. Fujimori, J. Magn. Magn. Mater. 47 (1985) 243–247.
[26] C. Kern, P.M. Raccah, J. Phys. Chem. Solids 26 (1965) 1625–1628.
[27] T. Sakai, G. Adachi, J. Shiokawa, Solid State Commun. 40 (1981) 445–449.
[28] J.C. Nickerson, R.M. White, J. Appl. Phys. 40 (1969) 1011–1012.
[29] C. Kittel, Introduction to Solid State Physics, 5th ed., John Wiley International Ltd., London, 1985.
[30] M. Faticanti, N. Cioffi, S. De Rossi, N. Ditaranto, P. Porta, L. Sabbatini, T.B. Zacheo, Appl. Catal. B: Environ. 60 (2005) 73–82.
[31] A.J. Dyakonov, C.A. Little, Appl. Catal. B: Environ. 67 (2006) 52–59.
[32] M. F-García, A. M-Arias, A. I-Juez, A.B. Hungría, J.A. Anderson, J.C. Conesa, J. Soria, Appl. Catal. B: Environ. 31 (2001) 39–50.
[33] E. Bekyarova, P. Fornasiero, J. Kaspar, M. Graziani, Catal. Today 45 (1998) 179–182.
[34] N.W. Cant, P.C. Hicks, B.S. Lenon, J. Catal. 54 (1978) 372–383.
[35] Y.Y. Y-Fang, J. Catal. 87 (1984) 152–162.
[36] J.M.D. Cónsul, I. Costilla, C.E. Gigola, I.M. Baibich, Appl. Catal. B: Environ. 339 (2008) 151–158.
[37] R.D. Monte, P. Fornasiero, J. Kaspar, P. Rumori, G. Gubitosa, M. Graziani, Appl. Catal. B: Environ. 24 (2000) 157–167.
[38] A.M. Pisanu, C.E. Gigola, Appl. Catal. B: Environ. 20 (1999) 179–189.
[39] J.H. Holles, M.A. Switzer, R.J. Davis, J. Catal. 190 (2000) 247–260.
[40] M. Schmal, M.A.S. Baldanza, M.A. Vannice, J. Catal. 185 (1999) 138–151.
[41] K. Nagaveni, G. Sivalingam, M.S. Hegde, G. Madras, Appl. Catal. B: Environ. 48 (2004) 83–93.
[42] M.A. Aramendía, V. Borau, J.C. Colmenares, A. Marinas, J.M. Marinas, J.A. Navío, F.J. Urbano, Appl. Catal. B: Environ. 80 (2008) 88–97.
[43] Ekaterina A. Kozlova, Alexander V. Vorontsov, Appl. Catal. B: Environ. 77 (2007) 35–45.
[44] J.C. Colmenares, M.A. Aramendía, A. Marinas, J.M. Marinas, F.J. Urbano, Appl. Catal. A: Gen. 306 (2006) 120–127.
[45] S. Mahapatra, G. Madras, T.N. Guru Row, Ind. Eng. Chem. Res. 46 (2007) 1013–1017.
[46] S. Roy, M.S. Hegde, Catal. Commun. 9 (2008) 811–815.